

Zero-delay Consistent and Smooth Trainable Interpolation

Emilio Ruiz-Moreno*, Luis Miguel López-Ramos*, *Member, IEEE*, and Baltasar Beferull-Lozano*[†], *Senior Member, IEEE*

*WISNET Center, Department of ICT, University of Agder, Grimstad, Norway

[†] SIGIPRO Department, Simula Metropolitan Center for Digital Engineering, Oslo, Norway

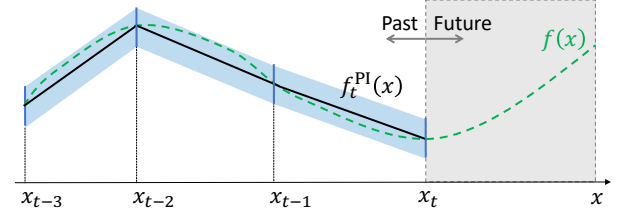
Abstract—The question of how to produce a smooth interpolating curve from a stream of uncertainty regions, which become available sequentially, is addressed in this paper. To this end, we formalize the concept of real-time interpolator (RTI): a trainable recurrent unit that reconstructs smooth signals that are consistent with the received uncertainty regions in an online manner. More specifically, an RTI works under the requirement of reconstructing a section of the signal immediately after an uncertainty region is revealed (zero delay), without changing the reconstructed signal in the previous sections. Particularly, this work formulates the design of spline-based RTIs and proposes a data-driven training procedure, which minimizes the average curvature of the interpolated signals over a set of example sequences. These sequences are representative of the nature of the data sequence to be interpolated, allowing to tailor the RTI to any specific signal source. Our overall design allows for different possible schemes due to its modular structure, but in this work, we present two approaches, namely, the parametrized RTI and the recurrent neural network (RNN)-based RTI, including their architectures and properties. Experimental results show that the two proposed RTIs can be trained to achieve improved performance (in terms of the curvature loss metric) with respect to a myopic-type RTI that only exploits the local information at each time step while maintaining smooth, zero-delay, and consistency requirements.

Index Terms—Online optimization, spline interpolation, recurrent neural networks, bi-level optimization.

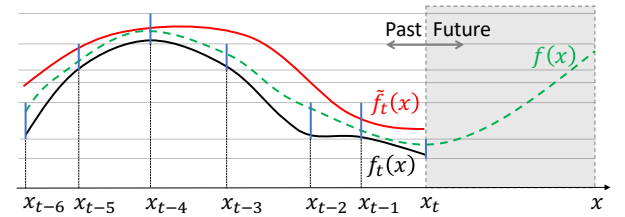
I. INTRODUCTION

Time series data are often transferred and stored in reduced or compressed forms. In several practical applications, such as industrial sensor data streams, data reduction schemes are based on non-uniform subsampling, where the samples to be eliminated are determined by the properties of the signal to be compressed.

One common motivation for applying data-reduction techniques is to allow efficient storing of collections of time series for a posterior analysis in batch form. In huge cyber-physical systems, the amount of information collected by pervasive sensors can be overwhelmingly large. In resource-constrained systems that can only retain the most recent data, discarding older data points can hinder the opportunity of learning in batch mode [1], [2]. An alternative to batch processing is online processing using techniques to learn from data in a streaming fashion [3]. Online learning allows extracting information from currently available data before it is discarded, and creates the opportunity to analyze streams of data generated



(a) The function f_t^{PI} denotes the current PI reconstruction. The blue shaded area represents the compression deviation over the PI reconstruction.



(b) The functions f_t and \tilde{f}_t represent a current consistent and non-consistent reconstruction, respectively.

Fig. 1: Example sequence of intervals of uncertainty obtained from an underlying signal f , by a PI compression mechanism, see Fig. 1a, and by a non-uniformly quantized and sampled acquisition, see Fig. 1b. The future is unknown to any of the reconstruction algorithms.

at high rates with the lowest delay possible in order to arrive at actionable intelligence [4].

Consider a practical scenario where several streams of sensor measurements are being collected and sent through a communication channel to a data center where they are consumed by machine learning algorithms that process data in streaming. If the communication channel is limited or expensive, a data reduction scheme must be applied at the sensory side, and a reliable decompression procedure must be executed at the receiver side where the reconstructed data stream is processed. An example of such a practical scenario is the collection of data from sensors in offshore oil and gas platforms and its transmission via satellite links to onshore data centers [5], [6].

In particular, the widespread PI system [7], [8], [9], [10] is a (lossy) data reduction technique that subsamples an input signal in a way such that the original time series can be approximately recovered by means of linear interpolation, with a reconstruction error guaranteed to be not larger than the

compression deviation (a user-tuneable parameter, see Fig. 1a).

Unlike linearly interpolated signals, many signals in physical systems are smooth [11], and a compression-decompression method that preserves the smoothness of the input signal is desirable. Moreover, since the compression deviation defines an uncertainty region where the original signal lies in, reconstruction methods that exploit such information are expected to yield more accurate signal reconstructions.

In this work, we seek online and smooth reconstruction methods of time series that are given as a sequence of interval values, from now on referred to as *interval data points*. Besides PI compressed signals, this type of data is found in several practical scenarios where a sensory acquisition system collects samples with an intrinsic uncertainty caused by the physical limitations of the sensors themselves or in acquisition systems that quantize the measurements [12], such as A/D converters. Both of them operating under a possibly non-uniform sampling (see Fig. 1b).

A. Related work

Penalized regression methods can be used to estimate an underlying signal either from noisy samples or uncertainty intervals by minimizing a weighted combination of a fitness measure and a regularization term that enforces a certain property, such as smoothness, in the reconstructed signal.

Kernel-based penalized regression approaches [13], [14], [15] and its online variants [16] allow to estimate complex signals by finding non-linear patterns at a moderate computational cost. Within the framework of streaming time series, sliding window-based methods have been proposed to improve the performance, with respect to a given metric, of the reconstructed signal (function estimate) by processing consecutive data points concurrently. As an example, the works [17] and [18] propose low-delay reconstruction algorithms by running a single processing iteration over a subsequence of interval data points, in a shifting window, every time a sample is received. Unfortunately, they are not able to guarantee that the reconstructed signal passes through all the interval data points, yielding a less reliable function estimate. Another challenge is that online kernel-based approaches propose a signal estimate whose complexity grows linearly with the number of samples. This is a direct consequence of the Representer Theorem [19], and it has two main drawbacks. First, the curse of kernelization [20], i.e., unbounded linear growth in model size and update time with the amount of data, making them dependent on complexity control mechanisms [21], [22]. The second drawback is the additive nature of the function estimate, which may modify the past reconstruction every time a new interval data point is processed, hence affecting the reliability of the function estimate. In [23], a technique for implementing causal interpolating kernels is proposed, which circumvents the issue of modifying past reconstructions; however, the proposed kernels have infinite support in the time domain, resulting in unbounded reconstruction complexity. Consequently, alternative approaches must be sought when, in addition to the smoothness and low-delay requirements, one needs to enforce constant model complexity and execution

time (with respect to the amount of data), while proposing function estimates that not only pass through all interval data points but also do not modify previous function estimates.

Interpolation techniques allow estimating a continuous signal within the range (set of values of the independent variable between its minimum and maximum) of the sampled interval data points. Various interpolation methods have been used since ancient times [24], but it was not until more recent centuries that its mathematical foundations were established [25]. Interpolation can be understood in two slightly different senses: i) *consistent* interpolation, where the estimate passes through all the interval data points; and ii) *smoothing* interpolation, where the estimate is enforced to be close to the data points, minimizing a certain fitting metric. In this paper, we focus on the first type of interpolation.

Some interpolation-based solutions have shown promising results in areas where the performance of the signal reconstruction depends on the quality of its function estimate under low-delay constraints, such as the online reconstruction of biosignals [26] or industrial manipulator trajectories [27], [28]. Among them, spline-based approaches [29], [30] can naturally accommodate smoothness requirements while being applicable in the field of real-time interpolation of streamed time-series data. As an example, the works [31], [32] aim at recovering the target signal by joining the centroids of every two consecutive data points. However, this type of procedure is not suitable in the scenario where the streamed data are in the form of intervals (e.g., quantization intervals). In addition, these methods do not let the user choose the order or the degree of smoothness [cf. Sec. II-C] of the spline.

Recent work has explored the use of recurrent neural networks (RNNs) in the context of signal interpolation. In particular, [33] addresses the problem of supervised learning from irregularly-sampled multivariate time series by means of a (semi-parametric) interpolation followed by an RNN. In the different but related context of learning under missing data samples, [34] develops several modified versions of the gated recurrent unit (GRU) [35], which account for missing samples in the input data. The aforementioned works combine an interpolation technique with an RNN to perform supervised learning. Distinctively, our work investigates the use of recurrent units for creating the ability to interpolate any two consecutive interval data points with a continuous (potentially up to any degree) polynomial function with low curvature and without knowing the subsequent data points.

B. Paper scope and contributions

This paper proposes a zero-delay spline-based interpolator specifically engineered to reconstruct signals from non-uniformly sampled interval data points given as intervals of possibly different length. This is accomplished by designing a recurrent cell (with its corresponding recurrent state) whose input is the current interval data point and whose outputs are the spline coefficients that conform the corresponding reconstructed signal section. In this work, we further analyze and exploit the relation between the recurrent cell and a parametric policy which maps the recurrent state into spline

coefficients. The structure of the policy is inherited from a parametric metric (or cost), which penalizes suboptimal decisions in the long term, hence improving the performance of the reconstruction under a zero-delay constraint. Moreover, by incorporating a policy within the recurrent unit, we can easily accommodate the continuity (smoothness) and consistency of the interpolation requirements in the reconstruction.

Due to its characteristics, our proposed method might be applied in the fields of audio, video, and communications, among others [36], [37].

The main contributions of this paper can be summarized as follows:

- We provide the formulation of a spline-based real-time interpolator (RTI) with zero-delay and which ensures consistency in the reconstruction (reconstructed signal samples pass through a given input sequence of intervals) while minimizing, at the same time, the expected curvature. Furthermore, our formulation allows the selection of both the order of the spline and its degree of smoothness.
- The solution to the RTI design problem is expressed as a recurrent unit that internally solves a parametrized optimization problem. To the best of our knowledge, our approach is the first one to formulate the online zero-delay interpolation in such a way. Due to the presence of the parametrized optimization problem within the RTI, the training problem must be formulated as a bi-level optimization problem. This is a direct consequence of accommodating the continuity and consistency constraints within a parametric policy that maps the recurrent unit state into spline coefficients.
- Due to the nature of splines, the RTI advantages are twofold: i) new signal estimates do not require to update the previous reconstruction, hence not affecting the hitherto reconstructed signal, and ii) a substantial reduction in the update time with respect to the amount of data, from linear to constant (as opposed to other popular methods, e.g. kernel methods without any model complexity control mechanism).
- We design two different RTI architectures, namely, the parametrized RTI, and the RNN-based RTI, including their properties and a procedure to train them from example data sequences. The training procedure allows also to train different RTIs tailored to different signal sources. To the best of our knowledge, there is no previous related work in the literature, so we have also designed a myopic RTI that only exploits local information at each time stamp, to be used as a benchmark.
- The proposed RTI design methodology is flexible enough to accommodate different alternative approaches (e.g. neural architectures) in addition to the two specific architectures proposed in the paper.
- We present experimental results where we have carried out training, validation and testing, showing the effectiveness of the two proposed RTIs, in terms of the curvature loss metric for both synthetic and real data.

The paper is structured as follows: Sec. II sets the notation and presents some basic concepts and definitions. Then, in Sec.

III, we formulate the problem addressed in this paper. Next, in Sec. IV and Sec. V, we respectively provide and validate a solution. Finally, Sec. VI concludes the paper.

II. PRELIMINARIES

In this section, we clarify the notation, introduce fundamental definitions and address some basic concepts that appear recurrently along the paper.

A. Notation

Vectors and matrices are represented by bold lowercase and bold capital letters respectively. Given a vector $\mathbf{v} = [v_1, \dots, v_D]^\top \in \mathbb{R}^D$, where $D \in \mathbb{N}$ denotes its dimensionality, its d th component is denoted as $[\mathbf{v}]_d \triangleq v_d$. Similarly, given a matrix $\mathbf{M} \in \mathbb{R}^{R \times C}$, the element in the r th row and c th column is denoted as $[\mathbf{M}]_{r,c}$. Finally, the notation $[\mathbf{v}]_{i:j}$ refers to the *sliced* vector $[v_i, \dots, v_j]^\top \in \mathbb{R}^{j-i+1}$.

B. Basic definitions

In this paper, we deal with streamed data in the form of sequential time-series conformed by intervals of uncertainty.

An interval \mathbf{l} is described by its time stamp $x \in \mathbb{R}$, centroid $y \in \mathbb{R}$ and half interval step size $\epsilon \in \mathbb{R}_+$, i.e., $\mathbf{l} = [x, y, \epsilon]^\top \in \mathcal{L} \subseteq \mathbb{R}^2 \times \mathbb{R}_+$. A set of intervals ordered in time is denoted here as a *sequence* where the t th interval is $\mathbf{l}_t = [x_t, y_t, \epsilon_t]^\top$. The interval-associated time stamps are set in strictly monotonically increasing order, i.e. $x_{t-1} < x_t$ for all time stamps in the sequence. Any two consecutive time stamps define a *time section* $\mathcal{T}_t = (x_{t-1}, x_t]$ with the exception of $\mathcal{T}_0 = \{x_0\}$. We denote a sequence of intervals as $\mathcal{Z} = \{\mathbf{l}_t\}_{t=0}^{|\mathcal{Z}|}$, where $|\mathcal{Z}|$ refers to its cardinality (or length).

1) *Curvature*: Let $\mathcal{F}_{\mathcal{D}}$ denote the space of continuous functions with first continuous derivative and second derivative square integrable, over the domain $\mathcal{D} \subseteq \mathbb{R}$. Then, we can define the (one-dimensional) curvature ([13], p.5) for any $f \in \mathcal{F}_{\mathcal{D}}$ as

$$\kappa(f) \triangleq \int_{\mathcal{D}} \left(\frac{d^2}{dx^2} f(x) \right)^2 dx = \int_{\mathcal{D}} \left(f^{(2)}(x) \right)^2 dx. \quad (1)$$

Intuitively, $\kappa(f)$ measures how far f is from having a linear behaviour.

2) *Consistency*: We adapt the term consistency from [38] as the property of any reconstructed signal falling into all intervals of a given sequence. Mathematically, f is a consistent reconstruction with respect to the sequence of intervals \mathcal{Z} if and only if $|f(x_t) - y_t| \leq \epsilon_t$ for all intervals in the sequence, i.e., $\forall t \in [0, |\mathcal{Z}|]$.

C. Spline

A spline is a piecewise-defined function where each piece or *function section* is a polynomial. Each function section contributes actively on its respective time section.

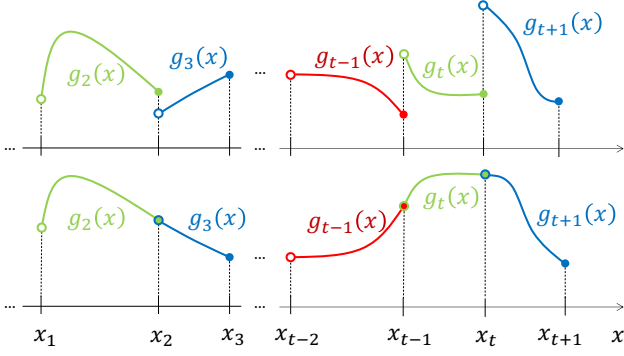


Fig. 2: Non-continuous spline vs. continuous spline. Same notation as in Sec. II-C.

Given a sequence of intervals \mathcal{Z} , its spline-based reconstruction can be expressed as

$$f_{|\mathcal{Z}|}(x) = \begin{cases} g_0(x), & \text{if } x = x_0 \\ g_1(x), & \text{if } x_0 < x \leq x_1 \\ \vdots & \\ g_{|\mathcal{Z}|}(x), & \text{if } x_{|\mathcal{Z}|-1} < x \leq x_{|\mathcal{Z}|} \end{cases} \quad (2)$$

where every function section $g_t : \mathcal{T}_t \rightarrow \mathbb{R}$ is a polynomial expressed as the linear combination

$$g_t(x) = \mathbf{a}_t^\top \mathbf{p}_t(x) \quad (3)$$

with combination coefficients $\mathbf{a}_t \in \mathbb{R}^{d+1}$ and the basis function vector $\mathbf{p}_t : \mathbb{R} \rightarrow \mathbb{R}^{d+1}$ set as

$$\mathbf{p}_t(x) = [1, (x - x_{t-1}), \dots, (x - x_{t-1})^d]^\top, \quad (4)$$

for all $x \in \mathcal{T}_t$. The parameter d denotes the *order* of the spline and it is user-defined in practice.

We say that a spline $f_{|\mathcal{Z}|}$ has a degree of *smoothness* φ , or equivalently that is of class C^φ , if it has φ continuous derivatives over the interior of its domain $\text{dom}(f_{|\mathcal{Z}|}) = \bigcup_{t=0}^{|\mathcal{Z}|} \mathcal{T}_t$. In order to compute the curvature of a spline $f_{|\mathcal{Z}|}$, as in (1), it must belong to the space $\mathcal{F}_{\bigcup_{t=0}^{|\mathcal{Z}|} \mathcal{T}_t}$. Every spline $f_{|\mathcal{Z}|}$ is compound by $|\mathcal{Z}| + 1$ function sections and $|\mathcal{Z}|$ contact points. We say that two consecutive function sections have a contact of order φ , at the union point, if they have φ equal derivatives. Clearly every t th function section g_t , defined over its time section \mathcal{T}_t , belongs to $\mathcal{F}_{\mathcal{T}_t}$. Hence, for $f_{|\mathcal{Z}|}$ to belong to $\mathcal{F}_{\bigcup_{t=0}^{|\mathcal{Z}|} \mathcal{T}_t}$ we additionally need to ensure that the contact points are at least of order $\varphi \geq 1$ (see Fig. 2).

In practice this can be enforced by imposing, at the contact points, the following equality constraint of continuity:

$$\lim_{x \rightarrow x_{t-1}^-} g_{t-1}^{(k)}(x) = \lim_{x \rightarrow x_{t-1}^+} g_t^{(k)}(x), \quad (5)$$

for every integer $k \in [0, \varphi]$ and $t \in [1, |\mathcal{Z}|]$, where the super index (k) denotes the k th derivative with respect to the time variable x .

Result 1. The constraint in (5) can be rewritten as

$$[\mathbf{a}_t]_{1:\varphi+1} = \mathbf{e}_t, \quad (6)$$

for every $t \in [0, |\mathcal{Z}|]$, where \mathbf{a}_t contains the combination coefficients of the t th function section, and $\mathbf{e}_t \in \mathbb{R}^{\varphi+1}$ is a vector such that each of its elements is defined as

$$[\mathbf{e}_t]_q = \frac{1}{(q-1)!} \sum_{i=1}^{d+1} [\mathbf{a}_{t-1}]_i u_{t-1}^{i-q} \prod_{j=1}^{q-1} (i-j), \quad (7)$$

where $u_t \triangleq x_t - x_{t-1}$, with the exception of \mathbf{e}_0 , which determines the initial conditions of the reconstruction and can be either calculated or set by the user.

See Appendix B for the derivation.

III. PROBLEM FORMULATION

With the definitions provided in Sec. II, we are ready to discuss the different ways to formulate the interpolation problem.

A. Batch interpolation

Given the whole sequence of intervals \mathcal{Z} , the function that consistently reconstructs the original signal with minimum curvature is the solution to the (batch) interpolation problem, formulated as

$$\begin{aligned} & \underset{f \in \mathcal{F}_{[x_0, x_{|\mathcal{Z}|}]}}{\text{minimize}} \quad \kappa(f) \\ & \text{subject to: } |f(x_t) - y_t| \leq \epsilon_t, \forall t \in [0, |\mathcal{Z}|], \end{aligned} \quad (8)$$

whose solution is known as the *natural cubic spline* [39]. The term cubic refers to a spline of order $d = 3$ with a degree of smoothness $\varphi = 2$, and it is termed natural because its second derivative equals zero at the contour points.

In order to solve an interpolation problem in batch form, all intervals must be available. However, in cases where interval data become available sequentially, a different approach is necessary. Moreover, a key observation is that the result of $d = 3$ and $\varphi = 2$ being optimal is no longer necessarily true.

The sequential case, implying working under the requirement that a function section is reconstructed right after each sample interval is received, is addressed in the ensuing section.

B. Online zero-delay interpolation

Consider the sequential setting in which the data samples of the sequence \mathcal{Z} become available one by one. Then, the goal is to create a *real-time interpolator* (RTI) that, once it receives the t th data sample, is required to reconstruct the signal segment within the new time section \mathcal{T}_t without affecting the previous reconstructed function sections. In addition, the resulting reconstructed signal f_t must be consistent with the sequence of intervals, and it must belong to $\mathcal{F}_{\bigcup_{i=0}^t \mathcal{T}_i}$.

When designing an RTI that has to act without knowledge of the ensuing interval data points, it will become necessary to interpret the interval sequence as a random process¹. Lastly, among all possible consistent reconstructed function candidates, the RTI must choose the one that reduces the expected curvature (over all possible sequences).

¹Since an exact characterization of the distribution of the interval sequence as a random process is generally impractical, in this paper a data-driven approach is adopted where only sample sequences are utilized [cf. Sec. III-D].

In this work, the focus is put on designing a spline-based RTI, employing a user-defined spline class of order $d \in \mathbb{N}$ and degree of smoothness $\varphi \in \mathbb{N}$ such that $1 \leq \varphi < d$. Note that if $\varphi = d$, the RTI becomes trivial, i.e., all the degrees of freedom are used to ensure the continuity. The reconstructed signal is built by adjoining function sections that satisfy the aforementioned constraints. When the RTI proposes a function section as in (3), it is underlyingly selecting the combination coefficients. Formally, the set of all these possible choices or *actions* is called *action space* and it is denoted as $\mathcal{A} \subseteq \mathbb{R}^{d+1}$. As soon as a vector of combination coefficients is chosen, the function section is determined because the basis vector is given, as in (4).

Due to the continuity constraint (5), an action taken after receiving a certain interval data point will have an impact on the function sections reconstructed in the future, hence on the overall curvature. This fact motivates for modeling the real-time interpolation problem in the context of sequential decision making over a state space.

We denote the state space as \mathcal{S} . Here, any t th state $\mathbf{s}_t \in \mathcal{S}$ has two components: a) the t th *input* (the last received interval, \mathbf{l}_t), and b) the t th *signal state*, denoted as $\boldsymbol{\sigma}_t$, in which the interpolation task was left at the previous iteration. The state update mechanism can be described by the mapping $F : \mathcal{S} \times \mathcal{A} \times \mathcal{L} \rightarrow \mathcal{S}$ as

$$\mathbf{s}_t = F(\mathbf{s}_{t-1}, \mathbf{a}_{t-1}, \mathbf{l}_t) := [\mathbf{l}_t^\top, \boldsymbol{\sigma}_t^\top]^\top, \quad (9)$$

where $\boldsymbol{\sigma}_t = [x_{t-1}, \mathbf{e}_t^\top]^\top$ is determined by (7) after taking an action. The signal state $\boldsymbol{\sigma}_t$ encodes the necessary information to ensure the φ degree of smoothness of the spline.

Actions will depend on the current state; therefore, designing an RTI is essentially designing a *policy*, i.e., a function defining how an RTI acts from a specific state. In this work, we focus on deterministic and stationary policies. Formally, a stationary policy can be described by a map $\pi : \mathcal{S} \rightarrow \mathcal{A}$. Particularly, we are interested in admissible (or feasible) actions, that is, a vector of combination coefficients that satisfy the continuity and consistency constraints. The set of all feasible actions, from a specific state, is defined as

$$\mathcal{A}(\mathbf{s}_t) \triangleq \{\mathbf{a} \in \mathcal{A} : [\mathbf{a}]_{1:\varphi+1} = \mathbf{e}_t, |\mathbf{a}^\top \mathbf{p}_t(x_t) - y_t| \leq \epsilon_t\}. \quad (10)$$

By extension, a feasible policy is a policy whose output is a feasible action for the corresponding input state. In the case of a deterministic and stationary feasible policy $\pi(\mathbf{s}_t) \in \mathcal{A}(\mathbf{s}_t)$. Finally, we refer to the set of all deterministic and stationary feasible policies as Π .

C. Concept of optimal policy

Among all policies $\pi \in \Pi$, the goal is to select the one that minimizes the curvature of the reconstructed signal. While in the batch case, the curvature minimization is a well-defined convex problem, in the sequential case, we have to rely on the expected curvature instead.

Before addressing the minimization of the expected curvature, we present two theorems that allow to write the objective function in a more convenient way.

Theorem 1 (Additivity). The curvature of a spline $f|_{\mathcal{Z}}$ described as in (2) can be computed additively as

$$\ddot{\kappa}(f|_{\mathcal{Z}}) = \sum_{t=1}^{|\mathcal{Z}|} \ddot{\kappa}(g_t). \quad (11)$$

Proof: see Appendix C.

Theorem 2 (Section curvature). Given a function section as defined in (3), its curvature can be computed as

$$\ddot{\kappa}(g_t) = \mathbf{a}_t^\top \mathbf{M}_t \mathbf{a}_t, \quad (12)$$

with $\mathbf{M}_t \in \mathbf{S}_+^{d+1}$ and

$$[\mathbf{M}_t]_{i,j} = \begin{cases} 0 & \text{if } i \leq 2 \text{ or } j \leq 2 \\ \frac{(i-1)(i-2)(j-1)(j-2)}{i+j-5} u_t^{i+j-5} & \text{otherwise,} \end{cases} \quad (13)$$

where $u_t \triangleq x_t - x_{t-1}$.

Proof: see Appendix D.

From **Theorem 1**, it is clear that the total curvature of a spline function is constructed by accumulating the curvature of each one of its function sections. Moreover, **Theorem 2** allows us to compute equivalently the curvature of any t th function section from the t th state and action as

$$\ddot{\kappa}(g_t) = \kappa(\mathbf{s}_t, \mathbf{a}_t) = \mathbf{a}_t^\top \mathbf{M}_t \mathbf{a}_t, \quad (14)$$

where \mathbf{M}_t is constructed from the information within the state \mathbf{s}_t . Specifically, from the current time stamp, x_t , corresponding to the input interval \mathbf{l}_t , and the previous time stamp, x_{t-1} , contained in the signal state $\boldsymbol{\sigma}_t$.

In this way, given initial state \mathbf{s}_0 (as the initial boundary condition) and following policy π , we can compute the total curvature as

$$J^\pi(\mathbf{s}_0) = \sum_{t=1}^{|\mathcal{Z}|} \kappa(\mathbf{s}_t, \pi(\mathbf{s}_t)). \quad (15)$$

As mentioned before, learning a policy involves minimizing the curvature in expectation over a random distribution of interval sequences. Then, the optimal policy, denoted by π^* , is defined mathematically as

$$\pi^* \triangleq \arg \min_{\pi \in \Pi} \mathbb{E}_{\mathcal{Z} \sim P_{\mathcal{Z}}} J^\pi(\mathbf{s}_0) \quad (16a)$$

$$\text{subject to: } \mathbf{s}_t = F(\mathbf{s}_{t-1}, \pi(\mathbf{s}_{t-1}), \mathbf{l}_t), \quad (16b)$$

for all $t \in [1, |\mathcal{Z}|]$, where $P_{\mathcal{Z}}$ denotes the probability distribution of sequences of interval data points.

D. Empirical optimization of the RTI

In general, the probability distribution $P_{\mathcal{Z}}$ introduced in (16) is unknown, thus computing any expectation with respect to it is not possible in practice. Therefore, in this work, we resort to the sample average approximation (estimating the expectation *empirically* as the average over a given set of training data). The aforementioned set of training data is constituted by M sequences as $\{\mathcal{Z}_m\}_{m=1}^M$.

Hence, instead of solving (16), we aim at solving the following data-driven surrogate optimization problem:

$$\tilde{\pi} \triangleq \arg \min_{\pi \in \Pi} \sum_{m=1}^M \frac{1}{|\mathcal{Z}_m|} \sum_{t=1}^{|\mathcal{Z}_m|} \mathbf{a}_{t,m}^\top \mathbf{M}_{t,m} \mathbf{a}_{t,m} \quad (17a)$$

$$\text{subject to: } \mathbf{s}_{t,m} = F(\mathbf{s}_{t-1,m}, \mathbf{a}_{t-1,m}, \mathbf{l}_{t,m}) \quad (17b)$$

$$\mathbf{a}_{t,m} = \pi(\mathbf{s}_{t,m}). \quad (17c)$$

Notice that the problem (17) involves minimizing over a space of functions and cannot be solved in practice unless it is restricted to a certain (smaller) family of policies in Π . The specific choice of policy will determine the type of RTI and hence, it will affect the performance of the solution.

IV. PROPOSED SOLUTION

In this section, we discuss how to design, evaluate, and train an RTI, in order to solve the problem of reconstructing a smooth signal from a sequence of interval data points under the zero-delay requirement.

A. Policy design

As mentioned in Sec. III-D, we are interested in reducing the policy space Π . To this end, in this paper we rely on a family of policies constructed via *parametric cost function approximation* (PCFA), a technique that searches into Π but rather than directly returning a feasible action it first solves a parametrized optimization problem over a constrained action space, [40]. Mathematically, given a spline of order d , degree of smoothness φ , and the t th state $\mathbf{s}_t = [\mathbf{l}_t^\top, \boldsymbol{\sigma}_t^\top]^\top$, our PCFA policy returns the t th action through

$$\mathbf{a}_t = \pi(\mathbf{s}_t; \boldsymbol{\theta}) \triangleq \arg \min_{\mathbf{a} \in \mathcal{A}(\mathbf{s}_t)} J(\mathbf{s}_t, \mathbf{a}; \boldsymbol{\theta}), \quad (18)$$

where $J : \mathcal{S} \times \mathcal{A} \times \mathbb{R}^P \rightarrow \mathbb{R}$ denotes the PCFA, which in our case can be understood as a metric used to penalize actions that lead to worse total curvatures and $\boldsymbol{\theta} \in \mathbb{R}^P$ is a vector containing P trainable parameters.

Specifically, the set of feasible actions at step t , $\mathcal{A}(\mathbf{s}_t)$, is a convex set. Therefore, we are interested in PCFAs that are strictly convex with respect to the optimization variable \mathbf{a} so that the problem (18) has a unique optimal solution. Moreover, it is computationally advantageous to design policies that can be evaluated in closed form, that is, (18) having a closed-form solution.

In order to capture the underlying distribution of sequences within the PCFA, a good insight into the structure of the problem is required. The policy design effort might be alleviated by incorporating more generic function approximators (such as neural networks) into the PCFA.

In this work, we describe three types of policies, which correspond to three possible forms of the PCFA in (18).

1) *Myopic policy*: The myopic policy chooses the feasible action that minimizes the *instantaneous* curvature at the t th time step, that is

$$J(\mathbf{s}_t, \mathbf{a}) = \mathbf{a}^\top \mathbf{M}_t \mathbf{a}, \quad (19)$$

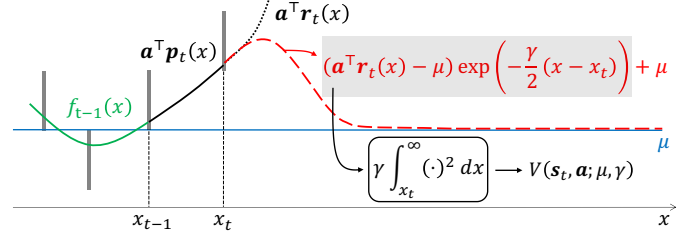


Fig. 3: Visualization of the cost-to-go interpretation for the parametrized policy. Only the terms within the gray shaded area pass through the integration block. The corresponding variables are defined in Sec. IV-A2.

where \mathbf{M}_t is given as in (13). Notice that the cost in (19) is invariant with respect to the trainable parameters contained in $\boldsymbol{\theta}$ and for clarity, we omit its dependency. The myopic policy is not expected to produce the best results but it will be used in the experimental Sec. V as a benchmark. Any other proposed policy must outperform the myopic policy to be deemed acceptable.

The myopic policy can be seen as a one-step lookahead policy whose cost-to-go has been set to zero. Notice that knowledge of the exact expected cost-to-go would enable enacting an optimal policy. However, complete knowledge of the distribution of interval sequences would be needed. We can still formulate policies relying on the *parametric* cost-to-go approximation [41], which is typically obtained by using prominent characteristics (features) of the state. Such features can be designed either by exploiting prior information about the problem at hand or in a data-driven fashion.

2) *Parametrized policy*: The parametrized policy chooses the feasible action that minimizes a weighted sum between the instantaneous curvature and a parametric cost-to-go function. The latter represents the deviation of future values of the interpolated signal from typical input intervals. Explicitly, the cost is defined as

$$J(\mathbf{s}_t, \mathbf{a}; \boldsymbol{\theta}) = \mathbf{a}^\top \mathbf{M}_t \mathbf{a} + \lambda V(\mathbf{s}_t, \mathbf{a}; \mu, \gamma), \quad (20)$$

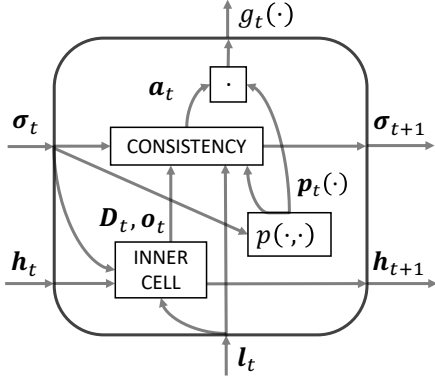
where $\boldsymbol{\theta} = [\mu, \gamma, \lambda]^\top \in \mathbb{R} \times \mathbb{R}_+^2$ and

$$V(\mathbf{s}_t, \mathbf{a}; \mu, \gamma) = \gamma \int_{x_t}^{\infty} (\mathbf{a}^\top \mathbf{r}_t(x) - \mu)^2 \exp(-\gamma(x - x_t)) dx, \quad (21)$$

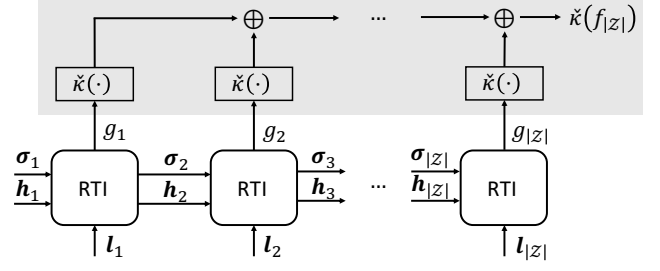
and where the vector-valued function $\mathbf{r}_t : \mathbb{R} \rightarrow \mathbb{R}^{d+1}$ is the *analytic continuation*² function of the basis vector (4) over the whole real line.

The main goal behind the cost-to-go (21) is to produce an interpolated signal in such a way that the spline remainder $\mathbf{a}^\top \mathbf{r}_t(x)$ is close to the average center of the interval samples that are about to come. For this purpose, we assume that the underlying process (generating the sequence \mathcal{Z}) is stationary. Then the parameter μ is meant to estimate the (time-invariant) mean of the process. Moreover, since interval data points lying further into the future barely affect the current action

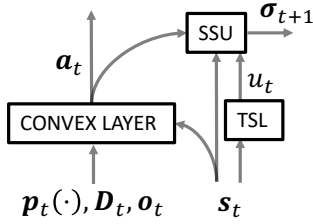
²Given a function defined analytically and restricted to a certain domain, its analytic continuation function is defined using the same equation and extending the domain to a superset of the original domain.



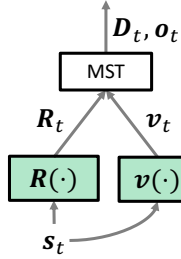
(a) Visualization of the internal architecture of an RTI unit.



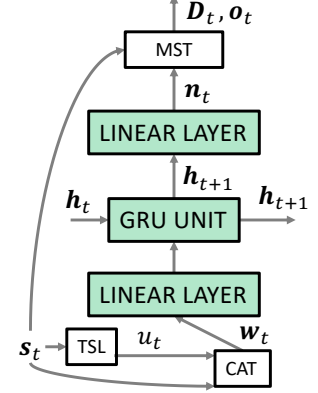
(b) Schematization of the unrolled RTI unit. The components under the gray area are only necessary during training.



(c) Consistency layer. The convex layer returns \mathbf{a}_t as (27) by solving (28).



(d) Architecture of the parametrized policy inner cell. The matrix \mathbf{R}_t and vector \mathbf{v}_t are computed as (23) and (24) respectively.



(e) Architecture of the RNN-based policy inner cell with $\mathbf{w}_t = [u_t, y_t, \epsilon_t, e_t^\top]^\top$. GRU unit refers to stacked GRU layers.

Fig. 4: The notation in the subfigures is the same as used in Sec. IV. The acronyms used refer to time section length (TSL), i.e., $u_t = x_t - x_{t-1}$, metric space transformation (MST), and signal state update (SSU). The CAT cell performs a concatenation. Cells containing trainable parameters are colored in green. Recall that $\mathbf{s}_t = [l_t^\top, \sigma_t^\top]^\top$.

we penalize the distance between the t th remainder and the estimated mean of the process, i.e., $\mathbf{a}^\top \mathbf{r}_t(x) - \mu$, starting from x_t , by weighting it with an exponential window with decay rate γ . Intuitively, splines whose remainders deviate more are more likely to incur higher overall curvature. This is because such deviation leads to disadvantageous starting conditions for the next function section. In order to obtain a bounded (finite) and positive metric of such a deviation, the distances are squared and integrated (see Fig. 3 for a visual representation).

Result 2. The cost-to-go of the parametrized policy, stated in (21), can be equivalently expressed as

$$V(\mathbf{s}_t, \mathbf{a}; \mu, \gamma) = \mathbf{a}^\top \mathbf{R}_t \mathbf{a} + \mathbf{a}^\top \mathbf{v}_t + \mu^2 \quad (22)$$

with

$$[\mathbf{R}_t]_{i,j} = \frac{(i+j-2)!}{\gamma^{i+j-2}} \sum_{k=0}^{i+j-2} \frac{(\gamma u_t)^k}{k!}, \quad (23)$$

and

$$[\mathbf{v}_t]_i = -2\mu \frac{(i-1)!}{\gamma^{i-1}} \sum_{k=0}^{i-1} \frac{(\gamma u_t)^k}{k!}. \quad (24)$$

See Appendix E for the derivation.

From **Result 2** and removing the terms that do not depend on the optimization variable in (18), we can equivalently rewrite the cost in (20) as

$$J(\mathbf{s}_t, \mathbf{a}; \lambda, \mu, \gamma) = \mathbf{a}^\top (\mathbf{M}_t + \lambda \mathbf{R}_t) \mathbf{a} + \lambda \mathbf{a}^\top \mathbf{v}_t. \quad (25)$$

Remark 1. The cost in (20) is convex with respect to \mathbf{a} . See appendix F for a proof.

3) *RNN-based policy:* The recurrent neural network (RNN)-based policy chooses the feasible action that minimizes a weighted sum between the instantaneous curvature and a parametric cost-to-go that penalizes the distance to the output of a certain RNN. Mathematically,

$$J(\mathbf{s}_t, \mathbf{a}; \theta) = \mathbf{a}^\top \mathbf{M}_t \mathbf{a} + \lambda \left\| \mathbf{a} - \begin{bmatrix} \mathbf{0}_{\varphi+1} \\ \mathbf{n}_t \end{bmatrix} \right\|_2^2, \quad (26)$$

where $\mathbf{n}_t \in \mathbb{R}^{d-\varphi}$ is the output of an RNN characterized by the function $N : \mathcal{S} \times \mathcal{H} \times \mathbb{R}^{P'} \rightarrow \mathbb{R}^{d-\varphi} \times \mathcal{H}$, such that $N(\mathbf{s}_t, \mathbf{h}_t, \theta') = [\mathbf{n}_t^\top, \mathbf{h}_{t+1}^\top]^\top$, where $\theta = [\lambda, \theta'^\top]^\top$ and $\mathbf{h}_t \in \mathcal{H}$ is its *latent* state. Notice that an RNN that successfully captures the temporal dynamics of the problem will pull towards actions that minimize the overall curvature.

TABLE I: Terms involved in each policy evaluation. See Appendix G for more details.

Myopic	
D_t	$B_2^\top M_t B_2$
\mathbf{o}_t	$-D_t^{-1} B_2^\top M_t B_1 \mathbf{e}_t$
Parametrized	
D_t	$B_2^\top (M_t + \lambda R_t) B_2$
\mathbf{o}_t	$-D_t^{-1} (B_2^\top (M_t + \lambda R_t) B_1 \mathbf{e}_t + \frac{1}{2} \lambda B_2^\top \mathbf{v}_t)$
RNN-based	
D_t	$B_2^\top (M_t + \lambda \mathbf{I}_{d+1}) B_2$
\mathbf{o}_t	$-D_t^{-1} (B_2^\top (M_t + \lambda \mathbf{I}_{d+1}) B_1 \mathbf{e}_t - \lambda \mathbf{n}_t)$

B. Policy evaluation

Evaluating the proposed policies, Sec. IV-A, consists in solving their related optimization problem, as in (18).

Result 3. The myopic policy, the parametrized policy, and the RNN-based policy admit a closed-form evaluation of the form

$$\mathbf{a}_t = \begin{bmatrix} \mathbf{e}_t \\ \boldsymbol{\alpha}_t \end{bmatrix}, \quad (27)$$

where $\boldsymbol{\alpha}_t \in \mathbb{R}^{d-\varphi}$ is computed as follows

$$\boldsymbol{\alpha}_t = \arg \min_{\boldsymbol{\alpha} \in \mathbb{R}^{d-m}} \|\boldsymbol{\alpha} - \mathbf{o}_t\|_{D_t}^2 \quad (28a)$$

$$\text{subject to: } |\boldsymbol{\alpha}^\top \mathbf{q}_t - z_t| \leq \epsilon_t, \quad (28b)$$

with $z_t = y_t - \mathbf{e}_t^\top [\mathbf{p}_t(x_t)]_{1:\varphi+1}$, $\mathbf{q}_t = [\mathbf{p}_t(x_t)]_{\varphi+2:d+1}$ and D_t and \mathbf{o}_t as in Table I. The optimization problem stated in (28) is commonly referred to as a *hyperslab* projection and admits a closed-form solution. For more details we refer to the Appendix G.

As discussed in Sec. III-B, designing an RTI is essentially designing a policy. At every time step t , the RTI proposes a function section depending on the current state. How such a state is updated depends on the input interval \mathbf{l}_t , and the previous action \mathbf{a}_{t-1} through the signal state $\boldsymbol{\sigma}_t$ [cf. (9)].

In this way, the dependencies between the RTI components resemble a *recurrent* cell or unit [42], (see Fig. 4a). All the trainable parameters, and the architecture that relates them, can be encapsulated in an inner cell while the continuity and consistency constraints are imposed through what we call a *consistency layer*. In fact, the consistency layer takes care of solving the convex optimization problem in (18), which is equivalent to evaluating a feasible action. In addition, the output of the consistency layer, which are the spline coefficients, can be differentiated with respect to the trainable parameters, categorizing this layer as a DCOL [43]. The closed-form evaluation offers a computational advantage with respect to general-purpose *differentiable convex optimization layer* (DCOL) tools such as CvxPyLayers [43], because its value and gradients are faster to calculate.

From this architecture point of view, the difference between the aforementioned proposed policies lies in the internal structure of the inner cell, while the DCOL is common to all of them. In the case of the myopic policy, the inner cell neither contains any trainable parameter nor uses a latent state.

As for the parametrized policy, the inner cell contains three parameters whose interactions have a high degree of associated interpretability, i.e., estimated mean of the process μ , window decay γ , and Pareto weight λ . Furthermore, it does not make use of a latent state either. Regarding the RNN-based policy, the inner cell consists in a recurrent unit, such as the well-established GRU or Long Short-term Memory (LSTM) unit [44], among others, which make use of a latent state.

Finally, notice that the scheme in Fig. 4a emphasizes the generalizability of the proposed approach. It can be noticed that alternative RTIs can be built depending on the problem at hand by simply modifying the DCOL and/or the inner cell.

C. Policy training

When we allude to the training of any of the proposed policies (see Sec. IV-A), we refer to solving the optimization problem stated in (17). Recall that we have restricted the policy space Π to a family of policies of the form given in (18). Thus, we can explicitly express the training procedure in terms of the following *bi-level* [45] optimization problem:

$$\min_{\boldsymbol{\theta} \in \mathbb{R}^P} \sum_{m=1}^M \frac{1}{|\mathcal{Z}_m|} \sum_{t=1}^{|\mathcal{Z}_m|} \mathbf{a}_{t,m}^\top \mathbf{M}_{t,m} \mathbf{a}_{t,m} \quad (29a)$$

$$\text{s. to: } \mathbf{s}_{t,m} = F(\mathbf{s}_{t-1,m}, \mathbf{a}_{t-1,m}, \mathbf{l}_{t,m}) \quad (29b)$$

$$\mathbf{a}_{t,m} = \arg \min_{\mathbf{a} \in \mathbb{R}^{d+1}} J(\mathbf{s}_{t,m}, \mathbf{a}; \boldsymbol{\theta}) \quad (29c)$$

$$\text{s. to: } |\mathbf{a}^\top \mathbf{p}_{t,m}(x_{t,m}) - y_{t,m}| \leq \epsilon_{t,m} \quad (29d)$$

$$[\mathbf{a}]_{1:\varphi+1} = \mathbf{e}_{t,m}. \quad (29e)$$

The inner-level optimization problem in (29) corresponds to (18), where the feasible-action constraint has been made explicit. Differently, the outer-level problem in (29) is a non-convex problem. For this reason we rely on gradient-based optimizers aiming to converge to a good high-performance local minimum.

Once a local minimizer for (29), denoted as $\tilde{\boldsymbol{\theta}}$, has been found, the complexity of reconstructing a sequence is only a forward pass per received interval data point: specifically, at step t , the corresponding spline coefficients are computed as $\mathbf{a}_t = \tilde{\pi}(\mathbf{s}_t) \triangleq \pi(\mathbf{s}_t; \tilde{\boldsymbol{\theta}})$. No iterative loops are required in the forward evaluation because all proposed RTI admit a closed-form evaluation (see Sec. IV-B).

As mentioned in Sec. IV-B, an RTI can be seen in general as a recurrent unit. Hence, reconstructing a sequence of interval data can be understood as an unfolded RNN and therefore, its parameters can be trained by means of back propagation through time (BPTT) [46], [47] (see Fig. 4b).

V. EXPERIMENT RESULTS

In this section, we experimentally validate the effectiveness of the proposed trainable RTIs. To this end, we explore different RTI architectures and make use of both synthetic and real data.

The performance of the reconstruction done by the RTIs under study is compared with that of a batch interpolator that knows the whole sequence in advance, and its curvature is therefore a lower bound.

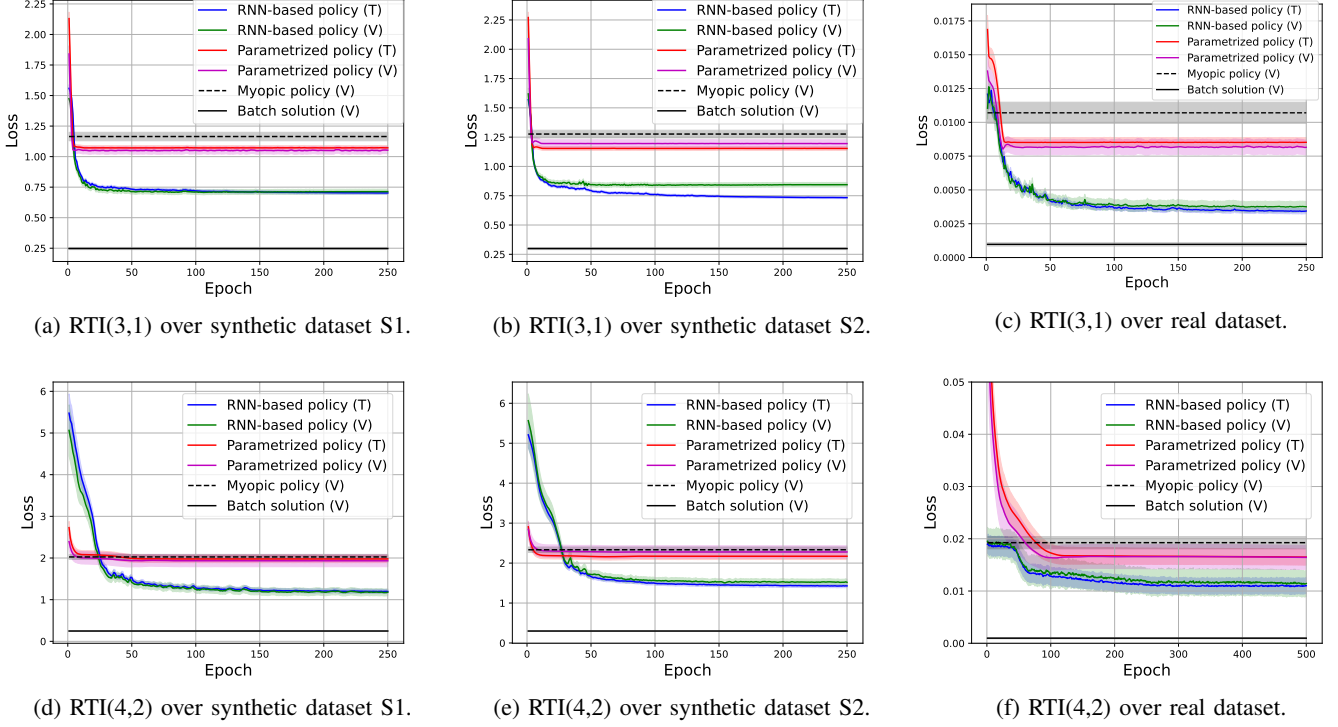


Fig. 5: Training and validation of proposed trainable RTI vs. the myopic policy and the batch solution for two different spline configurations. The legends (T) and (V) refer to training and validation datasets respectively. The notation $\text{RTI}(d, \varphi)$ refers to the order and degree of smoothness of the spline configuration. The loss is an unbiased estimate of the average curvature per function section. The shadow areas represent one standard deviation.

TABLE II: Testing of proposed RTI architectures. The notation (d, φ) refers to the order and degree of smoothness of the spline. The improvement is computed using the myopic loss as benchmark and the batch loss as baseline.

Spline Configuration	Policy	Dataset S1		Dataset S2		Real dataset	
		Loss	Improvement	Loss	Improvement	Loss	Improvement
(3,1)	Myopic	1.19 ± 0.05	-	1.32 ± 0.06	-	0.0097 ± 0.0010	-
	Parametrized	1.08 ± 0.05	$12.2\% \pm 7.4\%$	1.23 ± 0.05	$9.0\% \pm 7.0\%$	0.0083 ± 0.0009	$16.4\% \pm 13.2\%$
	RNN-based	0.74 ± 0.03	$48.2\% \pm 4.3\%$	0.84 ± 0.03	$46.8\% \pm 4.5\%$	0.0036 ± 0.0005	$69.1\% \pm 6.1\%$
(4,2)	Myopic	2.08 ± 0.10	-	2.40 ± 0.10	-	0.017 ± 0.002	-
	Parametrized	1.95 ± 0.26	$7.2\% \pm 15.4\%^*$	2.35 ± 0.20	$2.2\% \pm 11.8\%^*$	0.015 ± 0.003	$9.0\% \pm 18.5\%^*$
	RNN-based	1.22 ± 0.12	$47.1\% \pm 7.1\%$	1.53 ± 0.13	$41.4\% \pm 6.8\%$	0.010 ± 0.003	$44.8\% \pm 17.2\%$
	Batch	0.26 ± 0.01	-	0.31 ± 0.02	-	0.0008 ± 0.0001	-

A. Problem data

For these experiments we use two synthetic datasets and one real dataset. Each dataset consists of a time series of 28800 interval values which have been splitted into 288 sequences of 100 interval values each. Then, 192 sequences have been assigned to a training set, 64 to a validation set, and 32 to a test set, randomly. The benefits of this partition are three-fold: a) we can train the RTIs with a train-validation-test split, b) the RTI becomes more robust against unknown initial conditions, and c) we can validate the reconstruction against an optimal one (shorter sequences are computationally tractable using batch optimization).

Both of the synthetic datasets have been generated by first starting with a realization of a given autoregressive process AR(1), and then processing it to generate a sequence of

interval samples. Each sample in the original synthetic time series has been computed recurrently as $z_t = \phi z_{t-1} + w_t$, with autoregressive parameter $\phi = 0.9$ and Gaussian innovation $w_t \sim \mathcal{N}(0, 0.1)$.

The first synthetic dataset (S1) is a uniformly quantized and sampled time series. The centers of the quantization intervals have been computed with a uniform midtread quantizer as $y_t = \text{round}(z_t/2\epsilon_t)2\epsilon_t$ with a quantization half-step $\epsilon_t = 0.1$ for all t .

The second synthetic dataset (S2) has been obtained by compressing the aforementioned autoregressive time series with PI [7], with $\text{CompDev} = 0.1$, $\text{CompMax} = \infty$, and $\text{CompMin} = 0$. As a result, the samples' timestamps are not uniformly arranged anymore. The CompDev parameter is used as interval half-step, i.e., $\epsilon_t = 0.1$ for all t .

The real dataset (R1) is a univariate time-series measuring the pressure (bar) in an oil-separation deposit. The signal has been acquired with a uniform quantization half-step of 0.5 bar and, before compression, it was sampled every 5 s. Subsequently, it has been compressed by PI with a compression deviation equal to the quantization half-step of the acquisition process, resulting into a non-uniformly sampled sequence where the minimum time length between samples is 5 s.

B. RTI configurations

The choice of the spline order d and degree of smoothness φ has an impact on the interpolated signal that the RTI produces. In the case of the batch spline interpolation, any spline configuration where $d \geq 3$ and $\varphi \leq 2$ will result into a spline where $d = 3$ and $\varphi = 2$ (natural cubic spline). This fact motivates to try the configuration $(d = 3, \varphi = 2)$ with the RTI as long as there is no prior knowledge of the original signal (e.g., continuous acceleration). However, this configuration is unstable in a zero-delay scenario [48]. Therefore, we use in our experiments two low-order spline configurations that are stable under zero-delay: the first one $(d = 3, \varphi = 1)$ guarantees continuity in the first derivative, whereas the second one $(d = 4, \varphi = 2)$ guarantees continuity in the first and second derivatives of the spline reconstruction. Both chosen configurations can potentially perform as well as the batch solution. Notice that these configurations enjoy two degrees of freedom per function section, i.e., $d - \varphi = 2$.

In our experiment, for the RNN-based RTI inner cell, the GRU unit consists of 2 stacked GRU layers with an input size of 32 and a latent state of size 32.

C. Experiment setup and discussion

All datasets have been standardized with the mean and standard deviation of their corresponding training set. The benefits of this transformation are two-fold: a) the loss now depends entirely on the fluctuations of the values of the sequence (not on their magnitude), which helps to compare the performance over time-series of different nature, and b) the RNN-based RTI can improve its performance ignoring the magnitudes of the values and focusing on the fluctuations.

The proposed RTIs have been trained using the adaptive moments (Adam) optimizer [49] with $\beta_1 = 0.9$, $\beta_2 = 0.999$, without weight decay and learning rates 0.005 and 0.05 for the RNN-based and the parametrized configurations, respectively. The training has been carried out with mini-batches of 32 sequences and a learning rate scheduler that halves the base learning rate every 50 epochs. The training-validation curves are shown in Fig. 5.

As expected, the myopic policy performs better, on average, than the random initializations of the trainable RTIs, but once they are trained, the myopic is outperformed by them. The RNN-based policy achieves the best performance. However, it takes more epochs to converge³. These results are also

³Noticeably, the training of the RNN has taken a shorter wallclock time than that of the parametrized policy, despite the higher complexity of the RNN.

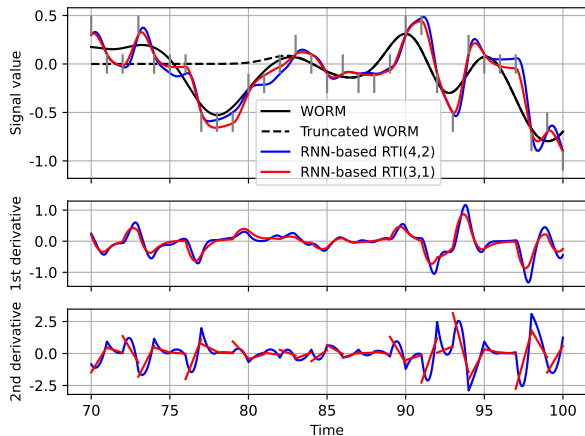


Fig. 6: Snapshot of a reconstructed time-series over a test sequence from dataset S1.

expected considering the reduced expressive representation capacity of the parametrized policy in comparison with the RNN-based one.

The results over the test datasets are summarized in Table II. They are also in agreement with the validation curves. It is worth mentioning that the parametrized policy for the configuration $(d = 4, \varphi = 2)$ does not outperform with statistical significance the myopic policy (these results are highlighted with an asterisk). To quantify the performance of a trainable RTI vs. the myopic benchmark, we use the batch solution as a baseline, such that an RTI achieving the same loss as the batch solution, would be reported as an *improvement* of 100% with respect to the myopic benchmark. The error in the improvement has been computed via error propagation from one standard deviation of each loss.

To illustrate that competing state-of-the-art online interpolation schemes do not fulfill the consistency constraints, we compare the RNN-based RTI, with spline configurations $(d = 3, \varphi = 1)$ and $(d = 4, \varphi = 2)$, with respect to the windowed online risk minimization (WORM) algorithm [18], an online kernel-based regression method design to track quantized signals. WORM and its truncated version have been configured with a Gaussian kernel of width 1.5, a window of 10 samples, a learning rate of 1 and a regularization parameter of 0.005. Fig. 6 shows a snapshot of one of the testing sequences of the dataset S1. Notice from Fig. 6 that WORM, with and without truncation, does not satisfy the consistency constraints. The derivatives of both of the WORM reconstructions have been omitted for clarity since a reconstruction using Gaussian kernels is infinitely differentiable. Lastly, comparing the curves in Fig. 6 corroborates the intuitive trade-off between low total curvature and a higher degree of smoothness. This can also be observed in the training-validation curves (Fig. 5a vs. 5d, 5b vs. 5e, 5c vs. 5f).

VI. CONCLUSION

In this paper we formalize the concept of RTI. Briefly, the RTIs are described as recurrent units that deal with irregular

sequences of non-uniform intervals of uncertainty. An RTI allows to consistently interpolate a sequence with zero delay, meaning that a function segment, covering up to the latest received time stamp, is produced immediately after the latest interval has been received. The experimental results in Sec. V show that both proposed architectures, namely the RNN-based and the parametrized RTI, outperform the (benchmark) myopic policy in average. These promising results motivate further development and experimentation with more elaborated architectures.

Finally, this work can be seen as a proof of concept with several immediate follow-ups. As a direct application, this work can be used to complement the PI system as a smooth decompression mechanism. Moreover, the design philosophy that was applied here for the RTI can be used to design an online joint compression-decompression scheme. The latter would involve mild modifications such as promoting sparsity.

Additionally, the close relationship between intervals of uncertainty and quantized signals encourages to study the error-decay of an RTI reconstruction as the sampling rate is increased while fixing the quantization step, or vice-versa [50]. This is novel in the sense that the RTI guarantees consistency under zero-delay requirements, which to the best of our knowledge, has not been deeply investigated to date.

Furthermore, the architecture of the RTI can be extended to deal with multivariate sequences of intervals of uncertainty, so that it does not only exploit temporal information of the data but also their spatial relations. A multivariate RTI architecture can be useful, for example, for real time trajectory planning, in the context of robotics [51], with the intervals of uncertainty describing safety regions along the trajectory.

APPENDIX

Proposition 1 (Positive (semi)-definiteness). Given a vector-valued real function $\mathbf{v} : \mathcal{D} \rightarrow \mathbb{R}^d$ with $\mathcal{D} \subseteq \mathbb{R}$, the matrix $\mathbf{W} \in \mathbb{R}^{d \times d}$ constructed as

$$[\mathbf{W}]_{i,j} = \int_{\mathcal{D}} [\mathbf{v}(x)]_i [\mathbf{v}(x)]_j dx, \quad (30)$$

is positive semi-definite. If additionally, the components of $\mathbf{v}(x)$ are linearly independent, then the matrix \mathbf{W} is positive definite.

A. Proof of Proposition 1

To prove positive semi-definiteness of \mathbf{W} , it suffices to prove that $\mathbf{z}^\top \mathbf{W} \mathbf{z} \geq 0$ for all $\mathbf{z} \in \mathbb{R}^d$. To this end, note that

$$\mathbf{z}^\top \mathbf{W} \mathbf{z} = \int_{\mathcal{D}} \mathbf{z}^\top \mathbf{v}(x) \mathbf{v}(x)^\top \mathbf{z} dx \quad (31a)$$

$$= \int_{\mathcal{D}} (\mathbf{z}^\top \mathbf{v}(x))^2 dx \geq 0. \quad (31b)$$

By definition, if the components of $\mathbf{v}(x)$ are linearly independent, there is no $\mathbf{z} \neq \mathbf{0}$ such that $\mathbf{z}^\top \mathbf{v}(x) = 0$ for $x \in \mathcal{D}$. Therefore, in this case, the inequality in (31b) is strict, meaning that \mathbf{W} is positive definite.

B. Derivation of Result 1

Recall, from (3), that the k th derivative of the t th function section can be computed as

$$g_t^{(k)}(x) = \mathbf{a}_t^\top \mathbf{p}_t^{(k)}(x) \quad (32)$$

and from (4), that the i th component of the t th basis vector equals

$$[\mathbf{p}_t(x)]_i = (x - x_{t-1})^{i-1} \quad (33)$$

for all $i \in [1, d+1]$. Therefore,

$$[\mathbf{p}_t^{(k)}(x)]_i = (x - x_{t-1})^{i-1-k} \prod_{j=1}^k (i-j), \quad (34)$$

for every $k \in [0, \varphi]$.

Now notice that

$$\lim_{x \rightarrow x_{t-1}^+} [\mathbf{p}_t^{(k)}(x)]_i = \begin{cases} k! & \text{if } i = k+1 \\ 0 & \text{otherwise.} \end{cases} \quad (35)$$

Hence,

$$\lim_{x \rightarrow x_{t-1}^+} g_t^{(k)}(x) = \sum_{i=1}^{d+1} [\mathbf{a}_t]_i \lim_{x \rightarrow x_{t-1}^+} [\mathbf{p}_t^{(k)}(x)]_i \quad (36a)$$

$$= k! [\mathbf{a}_t]_{k+1}. \quad (36b)$$

Thus, from (36) and defining the component

$$[\mathbf{e}_t]_{k+1} \triangleq \frac{1}{k!} \lim_{x \rightarrow x_{t-1}^+} g_{t-1}^{(k)}(x) \quad (37a)$$

$$= \frac{1}{k!} \sum_{i=1}^{d+1} [\mathbf{a}_{t-1}]_i (x_{t-1} - x_{t-2})^{i-1-k} \prod_{j=1}^k (i-j), \quad (37b)$$

we rewrite the equality in (5) as in (6). This is done by dividing both sides of the equality (5) by $k!$ and renaming the vector component index $k+1$ as q .

C. Proof of Theorem 1

Given a spline $f_{|\mathcal{Z}|}$, reconstructed from a sequence \mathcal{Z} as in (2), notice that $\text{dom}\{f_{|\mathcal{Z}|}\} = \bigcup_{t=0}^{|\mathcal{Z}|} \mathcal{T}_t$ and therefore, its curvature can be equivalently computed as

$$\kappa(f_{|\mathcal{Z}|}) = \int_{\bigcup_{t=0}^{|\mathcal{Z}|} \mathcal{T}_t} [f_{|\mathcal{Z}|}^{(2)}(x)]^2 dx \quad (38a)$$

$$= \int_{\mathcal{T}_1} [g_1^{(2)}(x)]^2 dx + \dots + \int_{\mathcal{T}_{|\mathcal{Z}|}} [g_{|\mathcal{Z}|}^{(2)}(x)]^2 dx \quad (38b)$$

$$= \sum_{t=1}^{|\mathcal{Z}|} \int_{\mathcal{T}_t} [g_t^{(2)}(x)]^2 dx \quad (38c)$$

$$= \sum_{t=1}^{|\mathcal{Z}|} \kappa(g_t). \quad (38d)$$

D. Proof of Theorem 2

The curvature of a function section, as in (3), can be computed as

$$\kappa(g_t) = \int_{\mathcal{T}_t} [g_t^{(2)}(x)]^2 dx \quad (39a)$$

$$= \int_{\mathcal{T}_t} [\mathbf{p}_t^{(2)}(x)^\top \mathbf{a}_t]^2 dx \quad (39b)$$

$$= \int_{\mathcal{T}_t} \mathbf{a}_t^\top \mathbf{p}_t^{(2)}(x) \mathbf{p}_t^{(2)}(x)^\top \mathbf{a}_t dx \quad (39c)$$

$$= \mathbf{a}_t^\top \mathbf{M}_t \mathbf{a}_t, \quad (39d)$$

with

$$[\mathbf{M}_t]_{i,j} = \int_{\mathcal{T}_t} [\mathbf{p}_t^{(2)}(x)]_i [\mathbf{p}_t^{(2)}(x)]_j dx. \quad (40)$$

Recall, from (34), that the second derivative with respect to time of the i th element of the basis function vector (4) is equal to

$$[\mathbf{p}_t^{(2)}(x)]_i = (i-1)(i-2)(x-x_{t-1})^{i-3}. \quad (41)$$

Thereby, it is clear by the relation in (41), that the first two rows and columns of the matrix \mathbf{M} are zero-valued. Letting $c = (i-1)(i-2)(j-1)(j-2)$ we can compute the remaining matrix components as

$$[\mathbf{M}_t]_{i,j} = c \int_{x_{t-1}}^{x_t} (x-x_{t-1})^{i-3} (x-x_{t-1})^{j-3} dx \quad (42a)$$

$$= c \int_0^{x_t-x_{t-1}} \tau^{i+j-6} d\tau \quad (42b)$$

$$= c \frac{(x_t-x_{t-1})^{i+j-5}}{i+j-5}. \quad (42c)$$

E. Derivation of Result 2

The upper incomplete gamma function is defined as

$$\Gamma(s, x) \triangleq \int_x^\infty t^{s-1} \exp(-t) dt. \quad (43)$$

It is worth to mention that when s is a positive integer then

$$\Gamma(s, x) = (s-1)! \exp(-x) \sum_{k=0}^{s-1} \frac{x^k}{k!}. \quad (44)$$

For the sake of clarity, we omit the dependencies in the notation. We restate the relation in (21) as

$$V = \gamma \int_{x_t}^\infty (\mathbf{a}^\top \mathbf{r}_t(x) - \mu)^2 \exp(-\gamma(x-x_t)) dx \quad (45a)$$

$$= \exp(-\gamma(x_{t-1}-x_t)) \cdot$$

$$\gamma \int_{x_t}^\infty (\mathbf{a}^\top \mathbf{r}_t(x) - \mu)^2 \exp(-\gamma(x-x_{t-1})) dx \quad (45b)$$

$$= \exp(\gamma u_t) \gamma \cdot$$

$$\int_{u_t}^\infty (\mathbf{a}^\top \hat{\mathbf{r}}_t(\tau) \hat{\mathbf{r}}_t(\tau)^\top \mathbf{a} - 2\mu \mathbf{a}^\top \hat{\mathbf{r}}_t(\tau) + \mu^2) \exp(-\gamma\tau) d\tau \quad (45c)$$

$$= \mathbf{a}^\top \mathbf{R}_t \mathbf{a} + \mathbf{a}^\top \mathbf{v}_t + \mu^2. \quad (45d)$$

We arrive to the expression in the step (45b) by adding the zero $x_{t-1}-x_{t-1}$ within the exponential and rearranging terms.

TABLE III: Form of the terms of the cost of each policy expressed as a quadratic objective.

	Myopic	Parametrized	RNN-based
\mathbf{A}_t	\mathbf{M}_t	$\mathbf{M}_t + \lambda \mathbf{R}_t$	$\mathbf{M}_t + \lambda \mathbf{I}_{d+1}$
\mathbf{b}_t	$\mathbf{0}_{d+1}$	$\lambda \mathbf{v}_t$	$-2\lambda [\mathbf{0}_{\varphi+1}^\top, \mathbf{n}_t^\top]^\top$

Then in the step (45c), we change the integration variable for $\tau = x - x_{t-1}$, denote $\hat{\mathbf{r}}_t(\tau) = [1, \tau, \dots, \tau^d]^\top$, $u_t = x_t - x_{t-1}$ and expand the terms under the square. Finally, the last step (45d) is obtained by evaluating the integral with

$$[\mathbf{R}_t]_{i,j} = \exp(\gamma u_t) \gamma \int_{u_t}^\infty [\hat{\mathbf{r}}_t(\tau)]_i [\hat{\mathbf{r}}_t(\tau)]_j \exp(-\gamma\tau) d\tau \quad (46a)$$

$$= \exp(\gamma u_t) \gamma \int_{u_t}^\infty \tau^{i+j-2} \exp(-\gamma\tau) d\tau \quad (46b)$$

$$= \exp(\gamma u_t) \gamma^{-i-j+2} \int_{\gamma u_t}^\infty \omega^{i+j-2} \exp(-\omega) d\omega \quad (46c)$$

$$= \exp(\gamma u_t) \frac{\Gamma(i+j-1, \gamma u_t)}{\gamma^{i+j-2}} \quad (46d)$$

$$= \frac{(i+j-2)!}{\gamma^{i+j-2}} \sum_{k=0}^{i+j-2} \frac{(\gamma u_t)^k}{k!}, \quad (46e)$$

where the step (46b) follows after substituting the i th element of the auxiliary vector valued remainder $[\hat{\mathbf{r}}_t]_i = \tau^{i-1}$. Next, we change the integration variable for $\omega = \gamma\tau$ yielding the step (46c). Lastly, the final step (46e), is obtained by making use of the result in (44).

Similarly, by applying the same steps

$$[\mathbf{v}_t]_i = -2\mu \exp(\gamma u_t) \gamma \int_{u_t}^\infty [\hat{\mathbf{r}}_t(\tau)]_i \exp(-\gamma\tau) d\tau \quad (47a)$$

$$= -2\mu \frac{(i-1)!}{\gamma^{i-1}} \sum_{k=0}^{i-1} \frac{(\gamma u_t)^k}{k!}. \quad (47b)$$

F. Correctness of Remark 1

The cost function in (25) is convex with respect to the optimization variable \mathbf{a} if the matrices \mathbf{M}_t and \mathbf{R}_t are positive semidefinite. This is due to, being $\lambda > 0$, the sum of such positive semidefinite matrices is positive semidefinite, and therefore the Hessian of the cost w.r.t. \mathbf{a} .

Both \mathbf{M}_t and \mathbf{R}_t defined in (40) and (46a) respectively, are positive semidefinite thanks to the **Proposition 1** and that γ and u_t are strictly positive.

G. Derivation of Result 3

Definition 1 (Auxiliary matrices). We define the matrices $\mathbf{B}_1 \triangleq [\mathbf{I}_{\varphi+1}, \mathbf{0}_{(\varphi+1) \times (d-\varphi)}]^\top \in \mathbb{R}^{(d+1) \times (\varphi+1)}$ and $\mathbf{B}_2 \triangleq [\mathbf{0}_{(d-\varphi) \times (\varphi+1)}, \mathbf{I}_{d-\varphi}]^\top \in \mathbb{R}^{(d+1) \times (d-\varphi)}$ for the sake of notation along the derivation.

It turns out that all three proposed policies can be evaluated by solving a quadratic convex problem of the form

$$\mathbf{a}_t = \arg \min_{\mathbf{a} \in \mathbb{R}^{d+1}} \mathbf{a}^\top \mathbf{A}_t \mathbf{a} + \mathbf{b}_t^\top \mathbf{a} \quad (48a)$$

$$\text{subject to: } |\beta^\top \mathbf{p}_t(x_t) - y_t| \leq \epsilon_t, \quad (48b)$$

$$[\beta]_{1:\varphi+1} = \mathbf{e}_t \quad (48c)$$

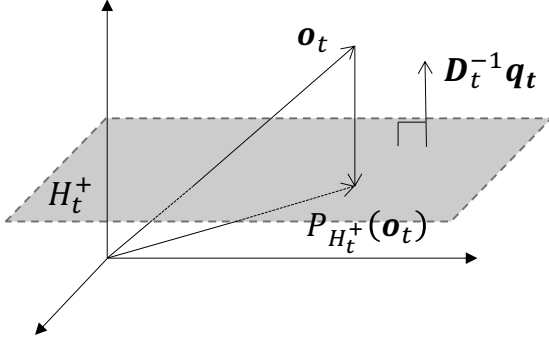


Fig. 7: Conceptualization of a hyperplane projection in the inner product space $(\mathbb{R}^{d-\varphi}, \langle \cdot, \cdot \rangle_{D_t})$ with $H_t^+ = \{u \in \mathbb{R}^{d-\varphi} : \langle u, D_t^{-1}q_t \rangle_{D_t} = z_t + \epsilon_t\}$.

where $A_t \in S_+^{d+1}$ and $b_t \in \mathbb{R}^{d+1}$ take different values depending on the policy. You can see them at Table III.

Notice that we can incorporate the equality constraint (48c) in the objective (48a) by restating

$$a = \begin{bmatrix} e_t \\ 0_{d-\varphi} \end{bmatrix} + \begin{bmatrix} 0_{\varphi+1} \\ \alpha \end{bmatrix}, \quad (49)$$

or equivalently, $a = B_1 e_t + B_2 \alpha$ where B_1 and B_2 are the auxiliary matrices in **Definition 1** and $\alpha \in \mathbb{R}^{d-\varphi}$. In this way, the optimization problem in (48) can be expressed as

$$a_t = \arg \min_{\alpha \in \mathbb{R}^{d-\varphi}} \alpha^\top B_2^\top A_t B_2 \alpha + (2e_t^\top B_1^\top A_t B_2 + b^\top B_2) \alpha \quad (50a)$$

$$\text{subject to: } |\alpha^\top q_t - z_t| \leq \epsilon_t, \quad (50b)$$

with $z_t = y_t - e_t^\top [p_t(x_t)]_{1:\varphi+1}$ and $q_t = [p_t(x_t)]_{\varphi+2:d+1}$.

On the other hand, given an inner product space $(\mathbb{R}^{d-\varphi}, \langle \cdot, \cdot \rangle_{D_t})$ with $D_t \in S_{++}^{d-\varphi}$ and inner product $\langle u_1, u_2 \rangle_{D_t} = u_1^\top D_t u_2$, for any $u_1, u_2 \in \mathbb{R}^{d-\varphi}$ and a vector $o_t \in \mathbb{R}^{d-\varphi}$, it is clear that

$$\|\alpha - o_t\|_{D_t}^2 = (\alpha - o_t)^\top D_t (\alpha - o_t) \quad (51a)$$

$$= \alpha^\top D_t \alpha - 2o_t^\top D_t \alpha + o_t^\top D_t o_t. \quad (51b)$$

Then, by identifying the terms, between the objective in (50a) and (51b), that depend on α we obtain the relations

$$D_t = B_2^\top A_t B_2 \quad (52)$$

and

$$o_t = -(B_2^\top A_t B_2)^{-1} \left(B_2^\top A_t B_1 e_t + \frac{1}{2} B_2^\top b_t \right) \quad (53)$$

allowing us to equivalently rewrite the optimization problem (50) as in (28).

The t th (closed) hyperslab, defined as the convex set

$$C_t \triangleq \{u \in \mathbb{R}^{d-\varphi} : |\langle u, D_t^{-1}q_t \rangle_{D_t} - z_t| \leq \epsilon_t\} \quad (54a)$$

$$= \{u \in \mathbb{R}^{d-\varphi} : |u^\top q_t - z_t| \leq \epsilon_t\}, \quad (54b)$$

can be visualized as the set of all points which belong between and onto the hyperplanes $H_t^+ = \{u \in \mathbb{R}^{d-\varphi} : u^\top q_t = z_t + \epsilon_t\}$ and $H_t^- = \{u \in \mathbb{R}^{d-\varphi} : u^\top q_t = z_t - \epsilon_t\}$.

Based on this observation, the projection onto the t th hyperslab $P_{C_t} : \mathbb{R}^{d-\varphi} \rightarrow \mathbb{R}^{d-\varphi}$ can be computed as

$$P_{C_t}(u) = \begin{cases} P_{H_t^+}(u) & \text{if } u^\top q_t > z_t + \epsilon_t \\ u & \text{if } |u^\top q_t - z_t| \leq \epsilon_t \\ P_{H_t^-}(u) & \text{if } u^\top q_t < z_t - \epsilon_t, \end{cases} \quad (55)$$

where $P_{H_t^+}$ and $P_{H_t^-}$ denote the projection onto the hyperplanes H_t^+ and H_t^- (see Fig. 7 as an example) given by

$$P_{H_t^+}(u) = u - (u^\top q_t - z_t - \epsilon_t) \frac{D_t^{-1}q_t}{q_t^\top D_t^{-1}q_t} \quad (56)$$

and

$$P_{H_t^-}(u) = u - (u^\top q_t - z_t + \epsilon_t) \frac{D_t^{-1}q_t}{q_t^\top D_t^{-1}q_t} \quad (57)$$

respectively.

Lastly, since the optimization problem (28) corresponds to a hyperslab projection, we can compute its solution by means of (55) as $\alpha_t = P_{C_t}(o_t)$.

Remark 2. D_t is invertible.

H. Correctness of Remark 2

From (40) we know that

$$M_t = \int_{\mathcal{T}_t} p_t^{(2)}(x) p_t^{(2)}(x)^\top dx. \quad (58)$$

Then,

$$B_2^\top M_t B_2 = \int_{\mathcal{T}_t} B_2^\top p_t^{(2)}(x) p_t^{(2)}(x)^\top B_2 dx. \quad (59)$$

Considering the way $B_2 \in \mathbb{R}^{(d+1) \times (d-\varphi)}$ is constructed (see **Definition 1**), we know that

$$B_2^\top p_t^{(2)}(x) = [p_t^{(2)}(x)]_{\varphi+2:d+1} \triangleq q_t^{(2)}(x), \quad (60)$$

with $p_t^{(2)}(x) \in \mathbb{R}^{d+1}$ and $q_t^{(2)}(x) \in \mathbb{R}^{d-\varphi}$. Thus,

$$z^\top B_2^\top M_t B_2 z = \int_{\mathcal{T}_t} z^\top q_t^{(2)}(x) q_t^{(2)}(x)^\top z dx \quad (61a)$$

$$= \int_{\mathcal{T}_t} (z^\top q_t^{(2)}(x))^2 dx > 0, \quad (61b)$$

for any $z \in \mathbb{R}^{d-\varphi}$. Notice that the inequality in (61b) holds because the components of $q_t^{(2)}(x)$ are linearly independent (polynomial of different degree), as shown in **Proposition 1**. For clarity, recall that from (41) and (60) we can explicitly write each component of $q_t^{(2)}(x)$ as

$$[q_t^{(2)}(x)]_i = (i + \varphi + 1)(i + \varphi)(x - x_{t-1})^{i+\varphi-1}. \quad (62)$$

Lastly, regardless of the chosen proposed policy, the matrix D_t consists of a sum of a positive definite and a positive (semi)-definite matrix, therefore D_t is positive definite and invertible.

REFERENCES

- [1] J. Gama, *Knowledge discovery from data streams*. CRC Press, 2010.
- [2] U. Sivarajah, M. M. Kamal, Z. Irani, and V. Weerakkody, "Critical analysis of big data challenges and analytical methods," *Journal of Business Research*, vol. 70, pp. 263–286, 2017.
- [3] J. Gama, "A survey on learning from data streams: current and future trends," *Progress in Artificial Intelligence*, vol. 1, no. 1, pp. 45–55, 2012.
- [4] A. A. Benczúr, L. Kocsis, and R. Pálovics, "Online machine learning in big data streams," *arXiv preprint arXiv:1802.05872*, 2018.
- [5] M. Mohammadpoor and F. Torabi, "Big data analytics in oil and gas industry: An emerging trend," *Petroleum*, vol. 6, no. 4, pp. 321–328, 2020.
- [6] M. reza Akhondi, A. Talevski, S. Carlsen, and S. Petersen, "Applications of wireless sensor networks in the oil, gas and resources industries," in *2010 24th IEEE International Conference on Advanced Information Networking and Applications*, pp. 941–948, IEEE, 2010.
- [7] OSIsoft, "Pi system," URL: <https://www.osisoft.com/pi-system>, 1980.
- [8] M. Cui, J. Zhang, A. R. Florita, B.-M. Hodge, D. Ke, and Y. Sun, "An optimized swinging door algorithm for identifying wind ramping events," *IEEE Transactions on Sustainable Energy*, vol. 7, no. 1, pp. 150–162, 2015.
- [9] F. Xiaodong, C. Changling, L. Changling, and S. Huihe, "An improved process data compression algorithm," in *Proceedings of the 4th World Congress on Intelligent Control and Automation (Cat. No. 02EX527)*, vol. 3, pp. 2190–2193, IEEE, 2002.
- [10] M. A. Khan, J. W. Pierre, J. I. Wold, D. J. Trudnowski, and M. K. Donnelly, "Impacts of swinging door lossy compression of synchrophasor data," *International Journal of Electrical Power & Energy Systems*, vol. 123, p. 106182, 2020.
- [11] O. Kosheleva and V. Kreinovich, "Why physical processes are smooth or almost smooth: A possible physical explanation based on intuitive ideas behind energy conservation," *Mathematical Structures and Modeling*, 2021.
- [12] R. M. Gray and D. L. Neuhoff, "Quantization," *IEEE transactions on information theory*, vol. 44, no. 6, pp. 2325–2383, 1998.
- [13] G. Wahba, *Spline models for observational data*. SIAM, 1990.
- [14] A. J. Smola and B. Schölkopf, *Learning with kernels*, vol. 4. Citeseer, 1998.
- [15] A. Nosedal-Sanchez, C. B. Storlie, T. C. Lee, and R. Christensen, "Reproducing kernel hilbert spaces for penalized regression: A tutorial," *The American Statistician*, vol. 66, no. 1, pp. 50–60, 2012.
- [16] J. Kivinen, A. J. Smola, and R. C. Williamson, "Online learning with kernels," *IEEE transactions on signal processing*, vol. 52, no. 8, pp. 2165–2176, 2004.
- [17] K. Slavakis, P. Bouboulis, and S. Theodoridis, "Online learning in reproducing kernel hilbert spaces," in *Academic Press Library in Signal Processing*, vol. 1, pp. 883–987, Elsevier, 2014.
- [18] E. Ruiz-Moreno and B. Beferull-Lozano, "Tracking of quantized signals based on online kernel regression," in *2021 IEEE 31st International Workshop on Machine Learning for Signal Processing (MLSP)*, pp. 1–6, IEEE, 2021.
- [19] G. Kimeldorf and G. Wahba, "Some results on tchebycheffian spline functions," *Journal of mathematical analysis and applications*, vol. 33, no. 1, pp. 82–95, 1971.
- [20] Z. Wang, K. Crammer, and S. Vucetic, "Breaking the curse of kernelization: Budgeted stochastic gradient descent for large-scale svm training," *The Journal of Machine Learning Research*, vol. 13, no. 1, pp. 3103–3131, 2012.
- [21] A. Singh, N. Ahuja, and P. Moulin, "Online learning with kernels: Overcoming the growing sum problem," in *2012 IEEE International Workshop on Machine Learning for Signal Processing*, pp. 1–6, IEEE, 2012.
- [22] A. Koppel, A. S. Bedi, K. Rajawat, and B. M. Sadler, "Optimally compressed nonparametric online learning: Tradeoffs between memory and consistency," *IEEE Signal Processing Magazine*, vol. 37, no. 3, pp. 61–70, 2020.
- [23] T. Blu, P. Thévenaz, and M. Unser, "High-quality causal interpolation for online unidimensional signal processing," in *2004 12th European Signal Processing Conference*, pp. 1417–1420, IEEE, 2004.
- [24] E. Meijering, "A chronology of interpolation: from ancient astronomy to modern signal and image processing," *Proceedings of the IEEE*, vol. 90, no. 3, pp. 319–342, 2002.
- [25] E. Waring, "Vii. problems concerning interpolations," *Philosophical transactions of the royal society of London*, no. 69, pp. 59–67, 1779.
- [26] O. Guven, A. Eftekhari, W. Kindt, and T. G. Constandinou, "Computationally efficient real-time interpolation algorithm for non-uniform sampled biosignals," *Healthcare technology letters*, vol. 3, no. 2, pp. 105–110, 2016.
- [27] S. A. Bazaz and B. Tondur, "Minimum time on-line joint trajectory generator based on low order spline method for industrial manipulators," *Robotics and Autonomous Systems*, vol. 29, no. 4, pp. 257–268, 1999.
- [28] T. Kröger, *On-Line Trajectory Generation in Robotic Systems: Basic Concepts for Instantaneous Reactions to Unforeseen (Sensor) Events*, vol. 58. Springer, 2010.
- [29] I. J. Schoenberg, "Contributions to the problem of approximation of equidistant data by analytic functions," in *IJ Schoenberg Selected Papers*, pp. 3–57, Springer, 1988.
- [30] L. Schumaker, *Spline functions: basic theory*. Cambridge University Press, 2007.
- [31] J. M. de Carvalho and J. V. Hanson, "Real-time interpolation with cubic splines and polyphase networks," *Canadian Electrical Engineering Journal*, vol. 11, no. 2, pp. 64–72, 1986.
- [32] R. Debski, "Real-time interpolation of streaming data," *Computer Science*, vol. 21, no. 4, 2020.
- [33] S. N. Shukla and B. M. Marlin, "Interpolation-prediction networks for irregularly sampled time series," *arXiv preprint arXiv:1909.07782*, 2019.
- [34] Z. Che, S. Purushotham, K. Cho, D. Sontag, and Y. Liu, "Recurrent neural networks for multivariate time series with missing values," *Scientific reports*, vol. 8, no. 1, pp. 1–12, 2018.
- [35] K. Cho, B. Van Merriënboer, C. Gulcehre, D. Bahdanau, F. Bougares, H. Schwenk, and Y. Bengio, "Learning phrase representations using rnn encoder-decoder for statistical machine translation," *arXiv preprint arXiv:1406.1078*, 2014.
- [36] Y. Liu, G. Wu, and Z. Zheng, "Seismic data interpolation without iteration using at-x-y streaming prediction filter with varying smoothness," *Geophysics*, vol. 87, no. 1, pp. V29–V38, 2022.
- [37] O. A. Agustín-Aquino, E. Lluis-Puebla, and M. Montiel, *Mathematics and Computation in Music: 6th International Conference, MCM 2017, Mexico City, Mexico, June 26-29, 2017, Proceedings*, vol. 10527. Springer, 2017.
- [38] I. Jovanovic and B. Beferull-Lozano, "Oversampled a/d conversion and error-rate dependence of nonbandlimited signals with finite rate of innovation," *IEEE Transactions on Signal Processing*, vol. 54, no. 6, pp. 2140–2154, 2006.
- [39] S. N. Wood, *Generalized additive models: an introduction with R*. CRC press, 2017.
- [40] W. B. Powell and S. Ghadimi, "The parametric cost function approximation: A new approach for multistage stochastic programming," *arXiv preprint arXiv:2201.00258*, 2022.
- [41] D. Bertsekas, *Reinforcement learning and optimal control*. Athena Scientific, 2019.
- [42] L. Medsker and L. C. Jain, *Recurrent neural networks: design and applications*. CRC press, 1999.
- [43] A. Agrawal, B. Amos, S. Barratt, S. Boyd, S. Diamond, and Z. Kolter, "Differentiable convex optimization layers," *arXiv preprint arXiv:1910.12430*, 2019.
- [44] S. Hochreiter and J. Schmidhuber, "Long short-term memory," *Neural computation*, vol. 9, no. 8, pp. 1735–1780, 1997.
- [45] E.-G. Talbi, "A taxonomy of metaheuristics for bi-level optimization," in *Metaheuristics for bi-level optimization*, pp. 1–39, Springer, 2013.
- [46] P. J. Werbos, "Backpropagation through time: what it does and how to do it," *Proceedings of the IEEE*, vol. 78, no. 10, pp. 1550–1560, 1990.
- [47] I. Goodfellow, Y. Bengio, and A. Courville, *Deep learning*. MIT press, 2016.
- [48] K. Erkorkmaz, "Efficient fitting of the feed correction polynomial for real-time spline interpolation," *Journal of Manufacturing Science and Engineering*, vol. 137, no. 4, 2015.
- [49] D. P. Kingma and J. Ba, "Adam: A method for stochastic optimization," *arXiv preprint arXiv:1412.6980*, 2014.
- [50] A. M. Powell and J. T. Whitehouse, "Error bounds for consistent reconstruction: Random polytopes and coverage processes," *Foundations of Computational Mathematics*, vol. 16, no. 2, pp. 395–423, 2016.
- [51] X. Li, Z. Sun, D. Cao, Z. He, and Q. Zhu, "Real-time trajectory planning for autonomous urban driving: Framework, algorithms, and verifications," *IEEE/ASME Transactions on mechatronics*, vol. 21, no. 2, pp. 740–753, 2015.